# <sup>19</sup>F Dynamic Nuclear Polarization at Fast Magic Angle Spinning for NMR of HIV-1 Capsid Protein Assemblies

Manman Lu<sup>1,2,3,#</sup>, Mingzhang Wang<sup>1,2,#</sup>, Ivan V. Sergeyev<sup>4,#</sup>, Caitlin M. Quinn<sup>1</sup>, Jochem Struppe<sup>4</sup>, Melanie Rosay<sup>4</sup>, Werner Maas<sup>4</sup>, Angela M. Gronenborn<sup>2,3\*</sup>, Tatyana Polenova<sup>1,2\*</sup>

<sup>1</sup>Department of Chemistry and Biochemistry, University of Delaware, Newark, Delaware 19716, United States; <sup>2</sup>Pittsburgh Center for HIV Protein Interactions, University of Pittsburgh School of Medicine, 1051 Biomedical Science Tower 3, 3501 Fifth Ave., Pittsburgh, PA 15261, United States; <sup>3</sup>Department of Structural Biology, University of Pittsburgh School of Medicine, 3501 Fifth Ave., Pittsburgh, PA 15261, United States; <sup>4</sup>Bruker Biospin Corporation, 15 Fortune Drive, Billerica, MA, United States

\*Corresponding authors: Angela M. Gronenborn, Department of Structural Biology, University of Pittsburgh School of Medicine, 3501 Fifth Ave., Pittsburgh, PA 15260, USA, Tel.: (412) 648-9959; Email: amg100@pitt.edu; Tatyana Polenova, Department of Chemistry and Biochemistry, University of Delaware, Newark, DE, USA, Tel.: (302) 831-1968; Email: tpolenov@udel.edu

Classification: Biological Sciences- Biophysics and Computational Biology

Keywords: magic angle spinning, <sup>19</sup>F NMR, HIV-1 capsid, dynamic nuclear polarization, DNP

<sup>\*</sup>These authors have contributed equally

## **ABSTRACT**

We report remarkably high, up to 100-fold, signal enhancements in <sup>19</sup>F dynamic nuclear polarization (DNP) magic angle spinning (MAS) spectra at 14.1 T on HIV-1 CA capsid protein assemblies. These enhancements correspond to absolute sensitivity ratios of 12-29 and are of similar magnitude as seen for <sup>1</sup>H signals in the same samples. At MAS frequencies above 20 kHz, it was possible to record 2D <sup>19</sup>F-<sup>13</sup>C HETCOR spectra, which contain long-range intra- and intermolecular correlations. Such correlations provide unique distance restraints, inaccessible in conventional experiments without DNP for protein structure determination. Furthermore, systematic quantification of the DNP enhancements as a function of biradical concentration, MAS frequency, temperature, and microwave power is reported. Our work establishes the power of DNP-enhanced <sup>19</sup>F MAS NMR spectroscopy for structural characterization of HIV-1 CA assemblies and this approach is anticipated to be applicable to a wide range of large biomolecular systems.

## INTRODUCTION

Magic angle spinning (MAS) NMR spectroscopy is a powerful tool for structural characterization of a wide range of biologically important materials, including protein assemblies and aggregates not amenable to other structural methods.<sup>1</sup> Atomic-resolution insights were recently gained by MAS NMR studies into poorly tractable systems, such as viral capsids,<sup>2-4</sup> microtubules,<sup>5</sup> actin and their associated proteins,<sup>6</sup> and aggregates of misfolded proteins.<sup>7,8</sup> Nevertheless, such studies still remain challenging because of low sensitivity and/or limited resolution, impeding widespread applications to large biological assemblies.

Dynamic nuclear polarization (DNP) is an attractive approach for sensitivity enhancement in NMR experiments, exploiting the transfer of polarization from electron spins to nuclear spins. <sup>9,10</sup> To that end, microwave irradiation is applied to saturate electron paramagnetic resonance (EPR) transitions, causing polarization transfer via several distinct mechanisms. <sup>11,12</sup> The theoretically attainable highest DNP enhancement factors, ε, are approximately equal to the ratio of gyromagnetic ratios of the electron to the nuclear spins; for the common biologically relevant atoms -- <sup>1</sup>H, <sup>13</sup>C, and <sup>15</sup>N -- these factors are ~660, 2,624, and 6,511, respectively. <sup>1</sup>H enhancements as high as 250 have been experimentally observed in biological solids. <sup>13</sup> In practice, transferring electron polarization in DNP-enhanced NMR spectroscopy requires the presence of paramagnetic centers in the samples. These can be endogenous paramagnetic groups <sup>14</sup> or externally introduced paramagnetic species. <sup>15</sup> Most commonly, samples are doped with suitable stable radicals or biradicals in an appropriate glass-forming matrix. <sup>15</sup>

DNP-enhanced MAS NMR spectroscopy of biological systems is an area of intense interest and active development, following in the footsteps of the seminal work from the Griffin group on bacteriorhodopsin and bacteriophages.  $^{16,17}$  With the availability of commercial instrumentation at magnetic fields of up to 21.1 T, DNP has since been applied to a variety of biological systems, including nanocrystalline peptides,  $^{18}$  membrane proteins,  $^{17}$  amyloid fibrils,  $^{19}$  nucleic acids,  $^{13}$  biomaterials,  $^{20-22}$  cells,  $^{23,24}$  and viral capsid assemblies.  $^{25,26}$  DNP enhancements were found to depend strongly on the detailed experimental conditions, such as magnetic field, temperature, nature and concentration of the radical, to name a few. Reported sensitivity gains for  $^{1}$ H polarization vary widely, from relatively modest factors of  $\varepsilon$ -4-10 for membrane proteins and at high magnetic fields of 18.8 T<sup>25</sup> to impressive  $\varepsilon$ -148 for direct  $^{13}$ C excitation in a perdeuterated microcrystalline SH3 protein. In our work on non-crystalline HIV-1 capsid tubular assemblies, we observed very large sensitivity gains of up to  $\varepsilon$ =64 at 14.1 T, permitting detection of resonances from dynamically disordered residues and low-concentration conformers, which are not observable in room-temperature MAS NMR experiments.

Yet, despite the exciting potential for applications of DNP-enhanced MAS NMR spectroscopy to biological systems, there are limitations preventing the widespread use of the technique. A significant challenge pertains to the severe deterioration of spectral resolution at cryogenic temperatures for a number of biological samples, 11,30 although rigid systems can exhibit narrow lines. 25,31,32 Low temperatures, typically below 120 K, are essential for attaining high DNP enhancements. Broadening of resonances is primarily inhomogeneous in nature, caused by the freezing-out of different conformations of low temperature sub-states, 4 and, to a lesser extent, due to the presence of paramagnetic radicals. Using temperatures in the 160-185 K range can to some degree alleviate the resolution loss. Unfortunately, in this temperature range, DNP sensitivity gains are considerably lower than those below 120 K. Indeed, the major impediment for routinely employing DNP on uniformly 13C, 15N-labeled large biomolecules is the limited resolution, and our work on HIV-1 capsid assemblies, where spectral overlap is severe for a number of residues, bears this out. 25

In order to address the resolution challenges and motivated by the potentially large sensitivity gains, we are exploring <sup>19</sup>F DNP-enhanced MAS NMR spectroscopy on several biological systems available in our laboratories. Here, we report on tubular assemblies of the HIV-1 CA capsid protein. These tubes are assembled from the 231-residue CA protein, which is the building block of mature HIV-1 conical capsids. The CA protein contains two independently folded, α-helical N- and C-terminal domains (NTD and CTD, respectively; Figure 1a). In virions, HIV-1 CA forms cone-like pleomorphic structures of varied shapes and appearances, 36 while in vitro, CA predominantly forms tubes (Figure 1b-d). Tubular CA assemblies have been extensively characterized experimentally by us and others using MAS NMR, 3,4,25,37-41 cryo-EM, 42-44 as well as computationally. 4,39,40,43 However, at present, an experimental atomic-resolution structure is not yet available. We recently showed that <sup>19</sup>F MAS NMR spectroscopy is a powerful technique for structural analysis of HIV-1 CA assemblies, 45 and the five tryptophan (Trp) residues in CA can conveniently be used for fluorine incorporation and exploited as effective reporters of structure. The <sup>19</sup>F MAS NMR spectrum of 5-fluorotryptophan (5F-Trp) labeled CA was readily assigned by mutagenesis, changing each Trp in turn to either Leu, lle or Tyr (Figure S1 of the Supporting Information). The resonance frequencies for all 5F-Trp resonances are distinct, reflecting their different local environments, and can be exploited for assessing conformational homo- or heterogeneity in these tubular assemblies. Remarkably, from F-F dipolar-based correlation spectra at MAS frequencies of 40-60 kHz, inter-fluorine distances as long as ~23 Å can be extracted. 45 While 19F solid-state NMR has been successfully used to investigate peptides and their interactions with membranes, 46-49 the dramatic benefits of 19F MAS NMR spectroscopy at frequencies exceeding 40 kHz to study biological systems have only recently been demonstrated. 45,50-52

For the <sup>19</sup>F DNP experiments described here, the CA protein was uniformly labeled with <sup>13</sup>C and <sup>15</sup>N as well as specifically labeled with 5F-Trp. Using AMUPol as the paramagnetic biradical, <sup>53</sup> DNP sensitivity enhancements up to 100 fold were observed in direct <sup>19</sup>F polarization experiments (Figure 2-3). These enhancements are remarkably high and of the same magnitude as the <sup>1</sup>H enhancements measured in the same CA tubular assemblies here and previously. <sup>25</sup> Under optimally designed experimental conditions, the strong DNP signals, combined with the high spectral resolution at MAS frequencies of 22-30 kHz, enabled us to record 2D <sup>19</sup>F-<sup>13</sup>C correlation experiments. These HETCOR spectra yield unique information about <sup>19</sup>F-<sup>13</sup>C intra- and intermolecular correlations corresponding to long-range distances. Therefore, they potentially complement the <sup>13</sup>C-<sup>13</sup>C and <sup>15</sup>N-<sup>13</sup>C experiments (as well as their proton-mediated versions), commonly used for deriving structural restraints for structure determination.

To the best of our knowledge, the work presented here is the first <sup>19</sup>F DNP-enhanced MAS NMR study of any biological system. Our results serve as proof-of-concept for the potential of this approach to probe structural features in proteins and large protein assemblies.

## **MATERIALS AND METHODS**

## Sample preparation

5-fuoroindole (Sigma Aldrich) was used as the precursor to uniformly incorporate fluorine at position 5 into all Trp residues of the HIV-1 CA protein. <sup>54</sup> 5-<sup>19</sup>F-Trp,U-<sup>13</sup>C, <sup>15</sup>N-labeled CA proteins were expressed and purified as reported previously with modifications. 38,55 In brief, 5-19F-Trp,U-<sup>13</sup>C, <sup>15</sup>N-labeled CA was expressed in modified M9 medium, containing 2 g of <sup>15</sup>NH₄Cl, 2 g of U-<sup>13</sup>C<sub>6</sub>-glucose and 20 mg of 5-fuoroindole per 1 L medium, using 0.8 mM IPTG for induction. Cells were grown at 18 °C and harvested after 16 h by centrifugation. Cell pellets were suspended in 25 mM sodium phosphate buffer (pH 7.0), ruptured by sonication on ice, and the cell debris was removed by centrifugation at 27,000 g at 4 °C for 1 h. The pH of the supernatant was adjusted to 5.8 with acetic acid and the conductivity was adjusted to below 2.5 ms/cm by dilution, followed by an additional centrifugation at 27,000 g at 4 °C for 1 h. The final supernatant was loaded onto a cation exchange column (HiTrap SP HP 5 mL, GE Healthcare) and the protein was eluted with a 0-1 M NaCl gradient in 25 mM sodium phosphate buffer (pH 5.8), 1 mM DTT, 0.02% NaN<sub>3</sub>. Fractions containing CA protein were pooled and further purified by gel filtration using a sizeexclusion column (HiLoad 26/600 Superdex 75 prep grade, GE Healthcare), equilibrated with 25 mM sodium phosphate buffer (pH 5.5), 1 mM DTT, 0.02% NaN<sub>3</sub>. Fractions containing CA protein were combined and concentrated to 30 mg/mL. 5-19F-Trp,U-13C,15N-labeled CA tubular assemblies were prepared from 30 mg/mL protein solutions in 25 mM phosphate buffer, 2.4 M NaCl (pH 6.5) by incubation at 37°C for 1 h and at 4°C overnight. 12.7 and 14 mg of protein were pelleted at 10,000 g and packed into two 1.9 mm thin-wall Bruker rotors.

For the DNP samples, we followed the general protocol established by us previously, with slight modifications. The biradical, AMUPol<sup>53</sup> was added to 11.0, 12.7, 14, 11.7, and 11.6 mg of pelleted tubes at a final concentration of 4.3, 12, 15, 22.8, and 28.2 mM. The pellets were gently stirred, until AMUPol dissolved and the color of the tubular assemblies turned light orange. 20% (v/v) glycerol-d<sub>8</sub> buffer containing 1 M NaCl was added on top, without disturbing the pellet, and the sample was incubated overnight at 4 °C. Excess glycerol solution was removed and the resulting DNP samples were pelleted at 10,000 g and packed into 1.9 mm Bruker rotors. The concentration of biradical AMUPol was measured by a Bruker benchtop EMXnano EPR spectrometer prior to DNP experiments.

Sample morphology was characterized by transmission electron microscopy (TEM). For the sample of tubular assemblies of 5-<sup>19</sup>F-Trp,U-<sup>13</sup>C, <sup>15</sup>N-CA, doped with 15 mM AMUPol, the images were acquired on a Zeiss Libra 120 transmission electron microscope operating at 120 kV. For the sample doped with 12 mM AMUPol, the images were acquired on a Talos F200C transmission

electron microscope operating at 200 kV, equipped with a Ceta 16 M camera. Assemblies were stained with uranyl acetate (0.5-1% w/v), deposited onto 400 mesh, formval/carbon-coated copper grids, and dried for 45 min in the air. The copper grids were glow discharged prior to staining, so that the tubular assemblies are uniformly spread on the grid surface and adhere to it.

## MAS NMR spectroscopy

<sup>19</sup>F and <sup>13</sup>C-detected MAS NMR experiments were recorded on a 19.96 T Bruker AVANCE III spectrometer, outfitted with 1.9 mm HX MAS probe. The Larmor frequencies were 850.4 MHz (<sup>1</sup>H), 213.8 MHz (<sup>13</sup>C), and 800.1 MHz (<sup>19</sup>F). The sample temperature was calibrated using KBr as a temperature sensor<sup>56</sup> and was maintained to ±1 °C throughout the experiments using a Bruker temperature controller.

The  $^{19}$ F and  $^{13}$ C-detected spectra were collected at the MAS frequency of 40 kHz at 290 K. The typical pulse lengths were 3.2  $\mu$ s for  $^{1}$ H, 3.9  $\mu$ s for  $^{13}$ C, and 3.2  $\mu$ s for  $^{19}$ F.  $^{1}$ H- $^{13}$ C cross-polarization (CP) was performed with a linear amplitude ramp (80–100%). The CP contact time was 0.7-1.2 ms. The  $^{13}$ C- $^{13}$ C correlation spectrum was acquired using RFDR<sup>57</sup> with a mixing time of 3.2 ms and  $^{1}$ H swfTPPM<sup>58</sup> decoupling (10 kHz).

<sup>19</sup>F chemical shifts were indirectly referenced to the adamantane-referenced <sup>13</sup>C chemical shifts.<sup>59</sup> 5-<sup>19</sup>F-DL-Trp powder was used as a secondary reference standard at -44.6 ppm (290 K). The <sup>1</sup>H, <sup>13</sup>C and <sup>15</sup>N chemical shifts were referenced with respect to DSS, adamantane and ammonium chloride as external referencing standards.

## <sup>19</sup>F DNP-enhanced MAS NMR spectroscopy

<sup>19</sup>F and <sup>1</sup>H DNP-enhanced MAS NMR experiments were performed in the Bruker Billerica laboratories on an Avance III HD SSNMR spectrometer, equipped with a 1.9-mm HXY(FXY) low temperature MAS probe, capable of irradiation at either <sup>1</sup>H or <sup>19</sup>F frequencies. At 14.1 T, the Larmor frequencies were 600.1 MHz (<sup>1</sup>H), 564.8 MHz (<sup>19</sup>F), and 150.9 MHz (<sup>13</sup>C). MW irradiation at a frequency of 395.18 GHz was generated by a second-harmonic gyrotron, capable of delivering in excess of 50 W irradiation at the sample. The dependence of intensity enhancement on the MW power was evaluated for 6.6 to 15.6 W. <sup>19</sup>F measurements were performed at 106 K, 109 K, 120 K, 125 K, 130 K, 160 K, and 185 K, with the sample temperature calibrated using KBr as a temperature sensor. <sup>56</sup> The actual sample temperature was determined using calibration curves of K<sup>79</sup>Br T<sub>1</sub>'s vs. the gyrotron power and stator temperature. The typical pulse lengths were 1.5 μs (<sup>1</sup>H), 1.25 μs (<sup>19</sup>F), and 2.5 μs (<sup>13</sup>C). <sup>19</sup>F spectra were acquired at MAS frequencies of 15 kHz, 20 kHz, 22 kHz, 24 kHz, 25 kHz, and 30 kHz, controlled by a Bruker MAS3 controller. <sup>1</sup>H DNP-enhanced spectra were acquired at 120 K and a MAS frequency of 24 kHz.

The  $^{19}\text{F-}^{13}\text{C}$  DNP HETCOR correlation spectra were acquired on the sample containing 15 mM AMUPol at the temperature of 120 K. MAS frequencies were 22 and 25 kHz and 90° pulse lengths were 3.0 µs ( $^{13}\text{C}$ ), and 1.25 µs ( $^{19}\text{F}$ ).  $^{19}\text{F-}^{13}\text{C}$  cross-polarization was achieved using rf fields of 108 kHz for  $^{19}\text{F}$  and 84 kHz for  $^{13}\text{C}$ ; a 10% tangential amplitude ramp was applied to  $^{19}\text{F}$ . HETCOR mixing times during the  $^{19}\text{F-}^{13}\text{C}$  cross-polarization step were 0.5, 1.5, 2.5, and 5 ms. All spectra were acquired as (2048 x 48) complex matrices with a recycle delay of 6 s and 128 transients for each  $t_1$  point, resulting in a total acquisition time of 10.24 hrs. States-TPPI phase sensitive detection was used for frequency discrimination in the indirect  $t_1$  dimension.

## Data processing and analysis

All spectra were processed in TopSpin and with NMRpipe, <sup>61</sup> and analyzed using Sparky. <sup>62</sup> For 2D <sup>13</sup>C-<sup>13</sup>C data sets, 60° or 90° shifted sine bell apodization, followed by Lorentzian-to Gaussian transformation were applied in both dimensions. The <sup>19</sup>F-<sup>13</sup>C HETCOR and <sup>19</sup>F-<sup>19</sup>F DQ-SQ spectra were processed with 90-degree phase shifted sinebell and Lorentzian-to-Gaussian apodization in the direct and indirect dimensions, respectively. Resonance assignments were based on available <sup>13</sup>C and <sup>19</sup>F chemical shifts of CA assemblies, <sup>38,39</sup> guided by and cross-checked against structural models. Assignments for particular cross peaks were deemed unambiguous if no other correlations were present at the corresponding (f<sub>2</sub>, f<sub>1</sub>) pair of frequencies or if only long-range correlations are possible. In the latter case, the cross peak was assigned to the correlation that corresponds to the shortest possible distance.

## **RESULTS AND DISCUSSION**

## **Spectral Resolution: Effect of AMUPol Biradical and Temperature**

<sup>19</sup>F MAS NMR spectra of tubular 5F-Trp,U-<sup>13</sup>C,<sup>15</sup>N-CA assemblies at 19.96 T and 290 K are displayed in Figure 2 (left panel). The chemical shifts range from -44.7 to -49.1 ppm and assignments were obtained via mutagenesis, as detailed in<sup>45</sup> and illustrated in Figure S1 of the Supporting Information. While this protocol requires preparation of several samples, which may be challenging in some systems, in general mutagenesis is significantly less difficult and time consuming than performing *de novo* overall resonance assignments, particularly in large proteins and protein assemblies, such as the HIV-1 CA assemblies studied here.

Doping of the sample with the AMUPol biradical does not interfere with the assembly (Figure 1d), but introduces broadening of one of the peaks, namely the signal at -47.3 ppm (Figure 2 bc). This peak comprises two resonances: the narrow W80 resonance, superimposed on the broad W184 signal. As illustrated in Figure 1b, W80 is located on the solvent exposed surface of the tube, while W184 is buried and resides at the intermolecular CTD-CTD dimer interface. Therefore, the most likely reason for the broadening of the W80 resonance is the proximity of the sidechain to the biradical AMUPol. We also note that the loss of the W80 resonance intensity and the reduction of the overall spectral resolution is more pronounced in the sample with 15 mM biradical, compared to the 12 mM AMUPol containing sample. The relative peak intensities and linewidths for the resolved resonances, W23, W117, and W133, are essentially identical to those in the biradical-free MAS NMR spectra. Only minor effects on the <sup>13</sup>C chemical shifts and line widths were induced by the presence of 12 mM AMUPol (Figure S2 and Table S1 of the Supporting Information). 37 resonances exhibit small intensity or chemical shift changes, with chemical shift perturbations ranging from 0.1 to 0.6 ppm. The largest effects are seen for the H84 and G89 resonances, which are associated with surface-exposed residues in the CypA-binding loop. These results indicate that the contribution of paramagnetic line broadening induced by the biradical is generally small at 290 K, consistent with previous studies.<sup>25</sup>

At cryogenic temperatures of 107 and 120 K, line broadening is dramatic (Figure 2; two right side panels). The <sup>19</sup>F spectrum is featureless and a single peak with a line width of ~8 ppm is detected. Broadening is also observed in the <sup>13</sup>C spectra at 120 K (Figures S3 and S4). The linewidths are 120-300 Hz, increase with increasing AMUPol concentration, and do not depend strongly on whether protons are decoupled or not. For comparison, at 290 K, the linewidths are 45-70 Hz. This is consistent with our previous observations in the 1D <sup>13</sup>C DNP spectra of HIV-1 CA assemblies.<sup>25</sup> In the future it will be desirable and necessary to systematically characterize the <sup>19</sup>F linewidths under DNP conditions in order to evaluate relative contributions of

homogeneous paramagnetic vs. inhomogeneous broadening. Such a study requires proton decoupling and fast MAS frequencies, currently not possible with the available DNP probe hardware.

## <sup>19</sup>F and <sup>1</sup>H DNP Buildup Times and Overall Enhancements

To systematically evaluate the <sup>19</sup>F DNP enhancement factors and buildup times, we examined their dependence on microwave power, temperature, MAS frequency, and AMUPol concentration. We chose to work with five concentrations of the AMUPol biradical, 4.3, 12, 15, 22.8, and 28.2 mM. In our prior work on HIV-1 CA assemblies, the AMUPol concentrations ranged from 8 to 10 mM.<sup>25</sup> Our findings are summarized in Table 1 and Figure 3 and discussed below.

*Microwave power.* The <sup>19</sup>F and <sup>1</sup>H DNP enhancements are very sensitive to the applied microwave power (Table 1 and Figure 3a,b). Signal saturation occurs at 13.8 W output power, where maximum gains and the fastest buildup times are observed. This condition was used for all 2D experiments.

Temperature. Temperature also has profound effects on the DNP enhancements, consistent with prior findings for all nuclei and all types of samples. <sup>12</sup> Increasing the temperature from 106 K to 185 K revealed a systematic decrease in the <sup>19</sup>F enhancement factors from 37 to 7 for the sample doped with 15 mM AMUPol (Table 1 and Figure 3c). Previous reports suggested that at temperatures of 160-185 K a suitable compromise is reached between the spectral resolution and sensitivity in <sup>13</sup>C-detected DNP experiments at 9.4 T.<sup>30</sup> This is not the case for <sup>19</sup>F DNP spectra as shown here: resolution is not regained under these conditions and the signal enhancements are prohibitively low (Figure 3c). Consequently, we chose to work at 120 K.

MAS frequency. Another key experimental variable is the MAS frequency, and MAS frequency dependence in DNP experiments remains poorly understood. Several conflicting reports exist and some suggest that the overall sensitivity in <sup>13</sup>C-detected CPMAS experiments drops systematically with increased spinning rates above 10 kHz,<sup>63</sup> and others showing only modest dependence on MAS and high enhancements at frequencies of 40 kHz.<sup>64-67</sup> For <sup>19</sup>F MAS NMR experiments conducted at temperatures above 0 °C, we recently demonstrated that fast MAS frequencies (40-60 kHz) are essential for obtaining high resolution. In addition, fast MAS frequencies alleviate the need for <sup>1</sup>H decoupling.<sup>52</sup> At present, the 1.9 mm probe suitable for DNP experiments can deliver MAS frequencies of up to 25 kHz, limiting our evaluation of higher frequencies. As illustrated in Figure 3a and summarized in Table 1, the highest integrated signal enhancements for the isotropic peak were observed at a MAS frequency of 20 kHz. The enhancements drop by ~10-17% at 22 kHz. At 15 kHz, the spinning sideband intensities are large,

since the reduced anisotropy of the <sup>19</sup>F CSA tensor is of the order of 44-46 ppm in the 5F-Trp-CA assemblies.<sup>45</sup> The integrated signal enhancement over the entire manifold of sidebands is 36 at this spinning frequency. Because of the large side band contributions, this condition is generally impractical for 2D <sup>19</sup>F-based correlation spectroscopy. The integrated signal enhancement associated with the isotropic peak is 32. Therefore, our results indicate that MAS frequencies of 20-25 kHz are optimal in terms of the sensitivity enhancements and averaging the <sup>19</sup>F CSA contribution.

Concentration of the AMUPol biradical. We and others have noted that different <sup>1</sup>H and <sup>13</sup>C DNP enhancement factors are measured in proteins and protein assemblies, even if very similar sample preparations are used.<sup>25</sup> It appears that the optimum biradical concentration depends on the details of the biological system under study, although in general concentrations of 6-50 mM seem to work satisfactorily (see a recent review<sup>12</sup>). For example, a study by Oschkinat and coworkers on proline demonstrated that it is necessary to carefully optimize the TOTAPOL concentrations in each sample for optimal sensitivity.<sup>68</sup> For increasing biradical concentrations, it has been reported that <sup>1</sup>H intensity enhancements increase and effective T<sub>1</sub> times decrease (both of which contribute to enhanced sensitivity). However, with growing biradical concentrations, line broadening also increases, while the number of detectable sites decreases, resulting in overall reduced sensitivity. It is therefore important to find the right balance between these effects for any new system, in order to achieve optimal sensitivity gains. The dependence of <sup>19</sup>F signal enhancements and the DNP buildup times on AMUPol biradical concentration is discussed below and compared to that for the <sup>1</sup>H signals.

*DNP signal buildup:* Buildup times of the <sup>19</sup>F and <sup>1</sup>H DNP signal intensities for the different samples and sets of experimental conditions are provided in Table 1. The <sup>19</sup>F polarization buildup time decreases with increasing temperature, from 18.6 s at 106 K to 11.3 s at 160 K, for the sample containing 15 mM AMUPol. Interestingly, the <sup>19</sup>F DNP buildup times are not strongly dependent on the AMUPol concentration: at 120 K, the buildup time constant (Tb) decreases from 11.8 s to 9.5 s when the AMUPol concentration is increased from 4.3 to 28.5 mM. In contrast, the buildup times for the <sup>1</sup>H DNP signals depend strongly on the AMUPol concentration, decreasing from 4.3 s to 0.9 s. Long buildup times generally impose long recycle delays in the DNP experiments. The optimal recycle delays for <sup>19</sup>F DNP experiments, where maximum sensitivity is attained per unit of time lie between 4 and 16 s (Table S2 of the Supporting Information). Therefore, we chose a recycle delay of 6 s in all 2D <sup>19</sup>F-<sup>13</sup>C HETCOR experiments, see below.

<u>DNP enhancements</u>: <sup>19</sup>F DNP MAS NMR single-pulse excitation spectra of 5F-Trp,U-<sup>13</sup>C, <sup>15</sup>N-CA tubular assemblies exhibit very large sensitivity gains, which grow with the increased AMUPol concentration, as shown in Table 1 and Figure 3d. At T = 120 K, a MAS frequency of 24 kHz, and AMUPol concentration of 4.3 mM, the signal enhancement, integrated over all sidebands, is 51 and 53 for microwave powers of 13.8 and 15.6 W, respectively. The largest enhancement factor of 100 is obtained for samples with 22.8 and 28.2 mM AMUPol.

Gratifyingly, these enhancements are similar to those for the  $^1$ H signals measured in the  $^1$ H-  $^{13}$ C DNP CPMAS spectra of identical samples, see Table 1 and Figure 3. The largest integrated  $^1$ H signal enhancement is 76-77, observed in the sample containing 4.3 mM AMUPol. Interestingly, the  $^1$ H enhancements do not depend strongly on biradical concentration. The values of the  $^1$ H enhancements measured here generally agree well with our previous findings in U-  $^{13}$ C,  $^{15}$ N- CA tubular assemblies, prepared with biradical concentrations of  $\sim$  8 mM, where 64-fold enhancements were observed at T = 109 K.  $^{25}$ 

The high <sup>19</sup>F enhancements observed here are remarkable and suggest that polarization transfer from the electrons to the fluorine nuclei (including in the buried sites) is highly efficient, despite the low number of fluorine sites (five) in the protein. This density of the <sup>19</sup>F sites is much lower than in any prior DNP studies utilizing protons, such as in our DNP investigations of HIV-1 CA assemblies reported here and previously, <sup>25</sup> and even when diluted by deuterium. <sup>29</sup> Hence, the <sup>19</sup>F-<sup>19</sup>F spin diffusion rates in the present study are expected to be much slower than those for the <sup>1</sup>H-<sup>1</sup>H spin diffusion. Indeed, this assertion is supported by the dependence of the DNP buildup times on the AMUPol concentration. The  $^{19}$ F Tb are 9.5 – 14.4 s at T = 120-125 K and depend only weakly on the biradical concentration. In contrast, the <sup>1</sup>H Tb are much shorter, 0.9 – 4.3 s, and exhibit a strong biradical concentration dependence. Taken together, these results indicate that <sup>19</sup>F DNP signal enhancements are not the result of a relayed effect. In the future it will be important to examine the contribution of spin diffusion to the <sup>19</sup>F DNP buildup rates and overall enhancements. This requires the preparation of several samples with a varying number of <sup>19</sup>F sites per molecule and/or per CA tube (e.g., by mixing the <sup>19</sup>F-labeled and nonfluorinated CA in different ratios prior to assembly), and/or the introduction of covalently linked biradical tags in close proximity to one of the <sup>19</sup>F sites such that the polarization transfer originates on a particular fluorine site and then propagates to the other sites through spin diffusion. Larger enhancements and shorter buildup times could potentially be obtained by the addition of fluorinated molecules in the polarization matrix, according to a recent study, 69 albeit this may be difficult to achieve in practice for aqueous protein preparations.

The absolute sensitivity ratios (ASR)<sup>70</sup> between the DNP-enhanced experiments at cryogenic temperatures and non-DNP experiments at 290 K were determined from the signal-to-

noise ratios relative to the maximum-intensity peak in the spectra, per unit of experiment time, per mg of sample. They lie in the range of 12-29, see Table S2 of the Supporting Information.

Taken together, the above results establish a range of favorable experimental conditions for <sup>19</sup>F DNP-enhanced MAS NMR experiments, taking into consideration currently available probe hardware. These conditions include temperatures of 106-120 K and MAS frequencies of 20-25 kHz and above. The optimum AMUPol concentration for these preparations is 4.3-12 mM, where a satisfactory compromise is achieved between high <sup>19</sup>F and <sup>1</sup>H enhancements, relatively short signal buildup times, and reasonably narrow <sup>13</sup>C lines.

## DNP-Enhanced <sup>19</sup>F-<sup>13</sup>C Heteronuclear Correlation Spectroscopy

DNP 2D  $^{19}$ F- $^{13}$ C HETCOR spectra acquired with mixing times of 0.5, 1.5, 2.5, and 5 ms are displayed in Figure 4. Such spectra would be very difficult to record without DNP enhancements at any temperature, given the low efficiency of  $^{19}$ F- $^{13}$ C cross polarization at room temperature (illustrated in Figure S5 of the Supporting Information for a  $^{19}$ F- $^{13}$ C CPMAS spectrum acquired at T = 290 K.). Based on the cross peak intensities, the polarization enhancement appears to be equally distributed between the different  $^{19}$ F sites.

Comparison between the different mixing time spectra reveals that many correlations are present in all data sets, although each spectrum contains unique information. Despite the limited resolution in the 1D <sup>19</sup>F and <sup>13</sup>C spectra at cryogenic-temperatures, the resolution of the HETCOR spectra at 120 K is sufficient to tentatively assign a number of cross peaks, based on the structural model of the CA protein (Table S3 of the Supporting Information). With increasing mixing times, more and longer-range correlations emerge. The longest distances for these correlations are 8 Å (0.5 ms), 11 Å (1.5 ms), 11 Å (2.5 ms), and 12 Å (5 ms). Mapping of the interactions around each 5F-Trp residue, based on the correlations in the DNP HETCOR spectra at different mixing times, onto the structure reveals similar size spheres around each F position (Figure 5).

In the spectrum acquired with a mixing time of 0.5 ms, a total of 36 <sup>19</sup>F-<sup>13</sup>C correlations were tentatively assigned. The majority of the cross peaks are associated with interactions between pairs of <sup>19</sup>F-<sup>13</sup>C nuclei separated by 4 to 8 Å (Table S4). Of these, 10 were assigned uniquely, 7 are two-fold ambiguous and the remaining ones are 3-fold ambiguous (Figure 4a). The majority of the cross peaks correspond to intramolecular correlations.

11 additional correlations are seen in the spectrum acquired with a 1.5 ms mixing time (Figure 4b). They were tentatively assigned to <sup>19</sup>F-<sup>13</sup>C pairs separated by 4 to 11 Å (Table S4). One-dimensional traces are provided in Figure S6 of the Supporting Information. Two cross peaks could be assigned uniquely, and three exhibit two-fold ambiguity. A further 11 new correlations

emerge in the 2.5 ms mixing time spectrum (consistent with <sup>19</sup>F-<sup>13</sup>C pairs at distances ranging from 4 to 11 Å). Two firm intramolecular assignments could be made (<sup>19</sup>F-<sup>13</sup>C pairs at distances of ~8 Å). Three additional cross peaks are two-fold ambiguous (Figure 4c). For the longest mixing time of 5 ms, 19 additional correlations appear (all intramolecular, <sup>19</sup>F-<sup>13</sup>C pairs at distances of 8 to 12 Å), 3 of which were assigned unambiguously and 4 possess two-fold ambiguity (Figure 4d).

It is important to note that the correlations observed in the <sup>19</sup>F-<sup>13</sup>C DNP-HETCOR spectra correspond to longer internuclear distances (up to 12 Å) than those observed in the <sup>13</sup>C-<sup>13</sup>C or <sup>13</sup>C-<sup>15</sup>N data sets, which report distances below 6-8 Å. While 3D structures of a number of proteins have been solved using <sup>13</sup>C-<sup>13</sup>C and <sup>13</sup>C-<sup>15</sup>N based distance restraints, <sup>5,7,71-75</sup> this approach alone does not yield satisfactory results for HIV-1 CA assemblies. For assembled CA and most multidomain proteins and large protein complexes, distance restraints beyond 8 Å are required to define the quaternary structure or supramolecular organization.

Taken together, the results discussed here are exciting and highlight the unique abilities of <sup>19</sup>F-<sup>13</sup>C DNP-enhanced correlation spectroscopy for providing unique long-range contacts that are difficult to measure via other biological MAS NMR experiments.

## CONCLUSIONS

The findings presented in this study underscore the exciting potential of <sup>19</sup>F DNP-enhanced MAS NMR spectroscopy to probe structural properties of protein assemblies, illustrated for HIV-1 capsid assemblies. The remarkably high signal enhancements observed in <sup>19</sup>F DNP spectra at MAS frequencies of 20-25 kHz permitted acquisition of 2D <sup>19</sup>F-<sup>13</sup>C correlation spectra, unattainable under conventional experimental conditions. The unique information content of these spectra, specifically the presence of numerous correlations that correspond to long-range distances, cannot be extracted from <sup>13</sup>C-<sup>13</sup>C or <sup>13</sup>C-<sup>15</sup>N correlation spectra. Thus, <sup>19</sup>F-based DNP HETCOR experiments represent a powerful addition to the protein structure analysis toolbox. We envisage that the approach presented here will have far-reaching applications in a wide range of large biological systems.

## **ACKNOWLEDGMENTS**

We thank In-Ja L. Byeon for acquiring <sup>19</sup>F solution NMR spectra of 5F-Trp, U-<sup>13</sup>C, <sup>15</sup>N CA and mutants. This work was supported by the National Science Foundation (NSF Grant CHE-1708773 to AMG and TP) and by the National Institutes of Health (NIGMS and NIAID, Grant P50 GM082251, Technology Development Project on MAS NMR). We acknowledge the National Science Foundation (NSF grant CHE-0959496) for the acquisition of the 850 MHz NMR spectrometer at the University of Delaware and the National Institutes of Health (NIH Grants P30GM103519 and P30GM110758) for the support of core instrumentation infrastructure at the University of Delaware. DNP resources were kindly provided by Bruker Biospin Corporation, Billerica, MA, USA.

## SUPPORTING INFORMATION AVAILABLE

<sup>19</sup>F solution NMR spectra of 5F-Trp, U-<sup>13</sup>C, <sup>15</sup>N CA and mutants; <sup>13</sup>C-<sup>13</sup>C RFDR spectra of tubular assemblies of 5F-Trp, U-<sup>13</sup>C, <sup>15</sup>N CA and 5F-Trp, U-<sup>13</sup>C, <sup>15</sup>N CA doped with 12 mM AMUPol; <sup>13</sup>C and <sup>19</sup>F MAS NMR spectra 5F-Trp, U-<sup>13</sup>C, <sup>15</sup>N CA in the presence of 12 mM AMUPol; resonance assignments in <sup>19</sup>F-<sup>13</sup>C DNP-enhanced HETCOR spectra. This information can be found on the internet at http://pubs.acs.org.

## **COMPETING FINANCIAL INTERESTS**

The authors declare no competing financial interests.

**Table 1.** Summary of <sup>19</sup>F and <sup>1</sup>H signal enhancements in 14.1 T DNP MAS NMR spectra of 5F-Trp,U-<sup>13</sup>C, <sup>15</sup>N CA tubular assemblies under different experimental conditions.\*

Biradical concentration (mM)	T (K)	MAS frequency (kHz)	Microwave power (mA / W**)	<sup>19</sup> F DNP polarization buildup time, Tb (s)	<sup>19</sup> F DNP signal enhancement		<sup>1</sup> H DNP	<sup>1</sup> H DNP signal enhancement
					integrated intensity (isotropic peak)	integrated intensity (all side bands)	polarization buildup time, Tb (s)	integrated intensity
4.3	120	24	120 / 8.4	11.8	29	37	4.3	63
			130 / 10.2		34	45		71
			140 / 12.0		38	48		76
			150 / 13.8		40	51		77
			160 / 15.6		41	53		76
12	120	15	150 / 13.8	11.1	32	36		
		20	130 / 10.2		68	70		
			150 / 13.8		77	82		
		22	130 / 10.2		50	60		
			150 / 13.8		66	72		
15	106		110 / 6.6	18.9	37	46		
	120	24	140 / 12.0		58.4	72		49
			150 / 13.8				1.4	50
	125	25	120 / 8.4	14.4	30	36		
			130 / 10.2		33	39		
			140 / 12.0		36	43		
			150 / 13.8		43	51		
			160 / 15.6		38	44		
	130	25	130 / 10.2		33	38		
	160	25	130 / 10.2	12.1	7	8		
	185	30	130 / 10.2		7	7		
22.2	120	24	150 / 13.8	10.9	79	100	1.2	72
28.5	120	24	150 / 13.8	9.5	80	98.5	0.9	65

\*The DNP enhancement factors were calculated as ratios of the integrated peak intensities for maximum peak intensities with and without the microwave irradiation.

\*\*Microwave power at the end of the waveguide.

# Figure 1

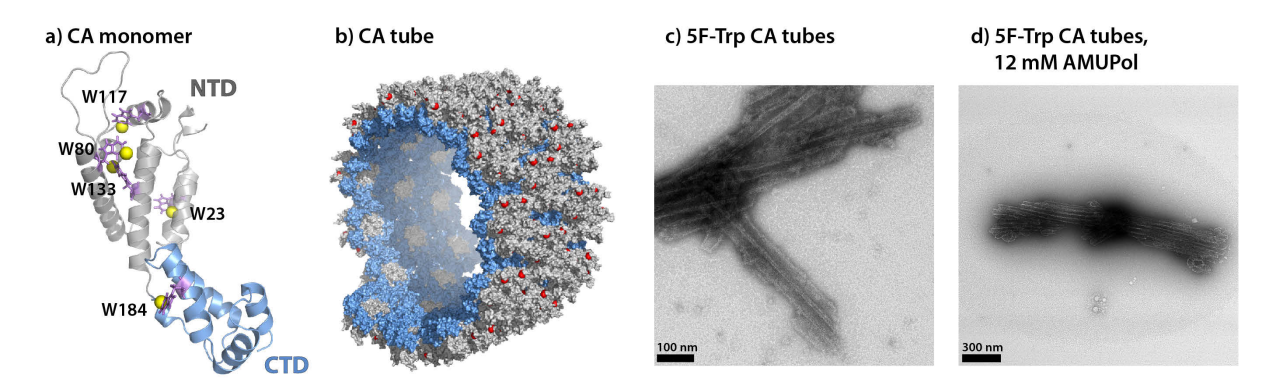


**Figure 1.** (a) Structure of HIV-1 CA monomer (PDBID: 4XFX). W23, W80, W117, W133 and W184 side chains are shown in purple stick representation with fluorine atoms as yellow spheres. (b) Section through the CA tube (PDBID: 3j4f). (c, d) Transmission electron micrographs of 5F-Trp,U-<sup>13</sup>C, <sup>15</sup>N-CA tubes in the absence (c) and presence (d) of 12 mM AMUPol. The scale bars are 100 nm and 300 nm, respectively.

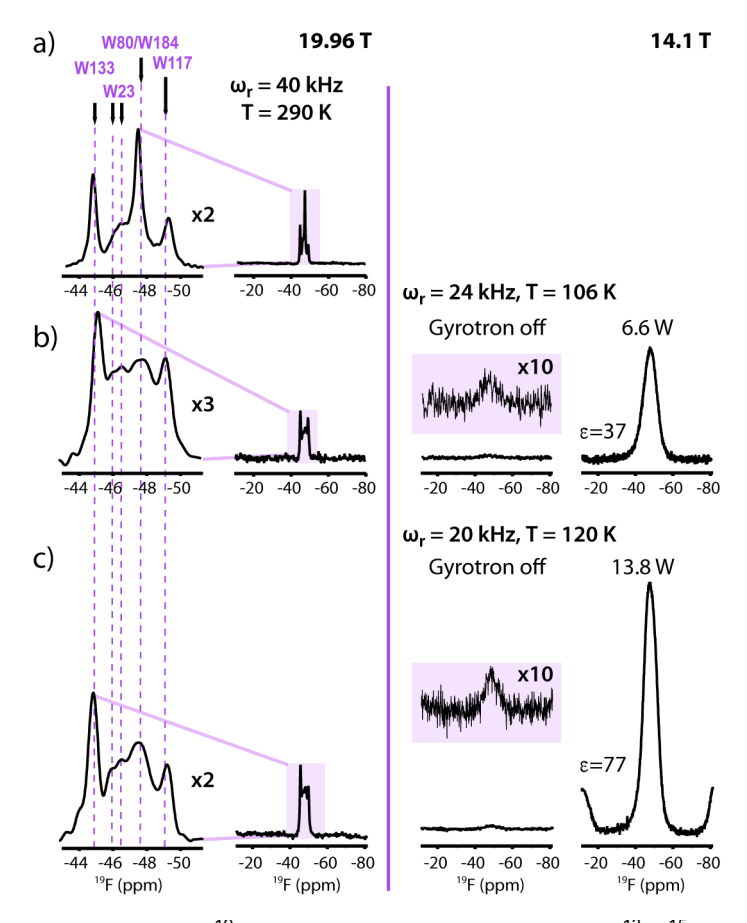


**Figure 2.** <sup>19</sup>F MAS and DNP-enhanced <sup>19</sup>F MAS NMR spectra of 5F-Trp,U-<sup>13</sup>C, <sup>15</sup>N CA assembled into tubes in the absence (a) and presence of 15 mM (b) and 12 mM AMUPol (c), respectively. The spectra in the left panel were acquired at 19.96 T (800.1 MHz <sup>19</sup>F Larmor frequency) at a MAS frequency of 40 kHz and 290 K. The spectra shown in the right panel were acquired at 14.1 T (564.8 MHz <sup>19</sup>F Larmor frequency) at MAS frequencies of 24 kHz and 20 kHz and temperatures of 106 K and 120 K, respectively. 16 scans and 48 scans were averaged for the spectra in the left and right panels, respectively. The DNP enhancements (maximum intensity: I<sub>MWon</sub>/I<sub>MWoff</sub>) were 36 (b) and 62 (c), respectively.

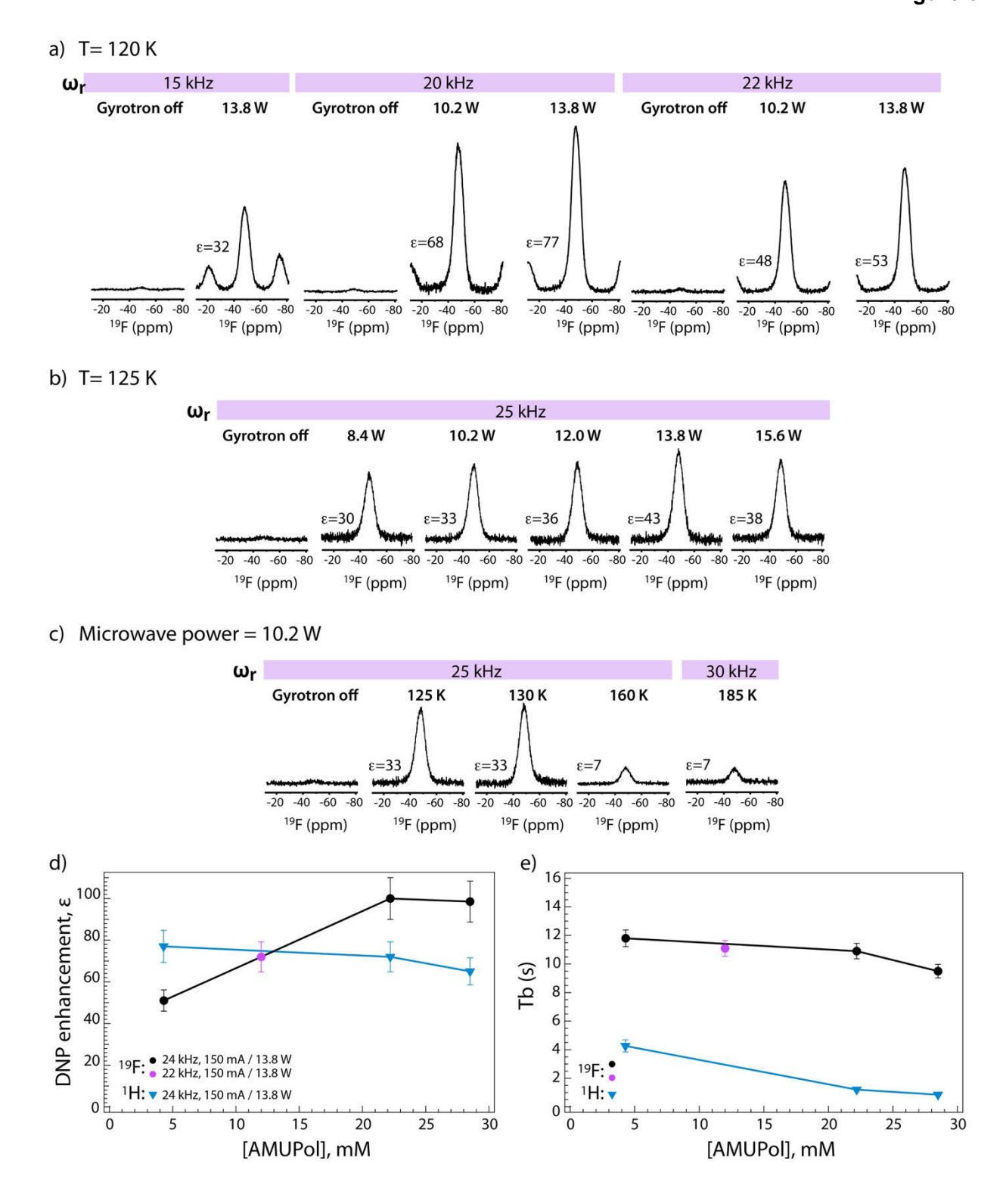


**Figure 3.** <sup>19</sup>F MAS and DNP-enhanced MAS NMR spectra of 5F-Trp,U-<sup>13</sup>C, <sup>15</sup>N CA, assembled into tubes in the presence of 12 mM (a) and 15 mM (b,c) AMUPol respectively. Spectra were acquired at 14.1 T (564.8 MHz <sup>19</sup>F Larmor frequency); the MAS frequencies, temperatures, microwave power, and DNP

enhancements for the integrated signal intensity of the isotropic peak are indicated next to each spectrum. 64 scans were averaged for the spectra in panel a), except for the spectrum recorded with a MAS frequency of 20 kHz and MW power of 10.2 W, which was acquired with 16 scans. 32 scans were averaged for all spectra in panels b), c), except for the 160 K spectrum, which was acquired with 440 scans. d), e) <sup>19</sup>F and <sup>1</sup>H DNP signal intensity enhancements, ε, and buildup time constants, Tb, for 5F-Trp,U-<sup>13</sup>C, <sup>15</sup>N CA tubular assemblies, plotted against AMUPol concentration. These data correspond to a sample temperature of 120 K, a MAS frequency of 24 kHz, and microwave power of 150 mA/13.8 W, except in d) for the samples containing 12 mM AMUPol (22 kHz).

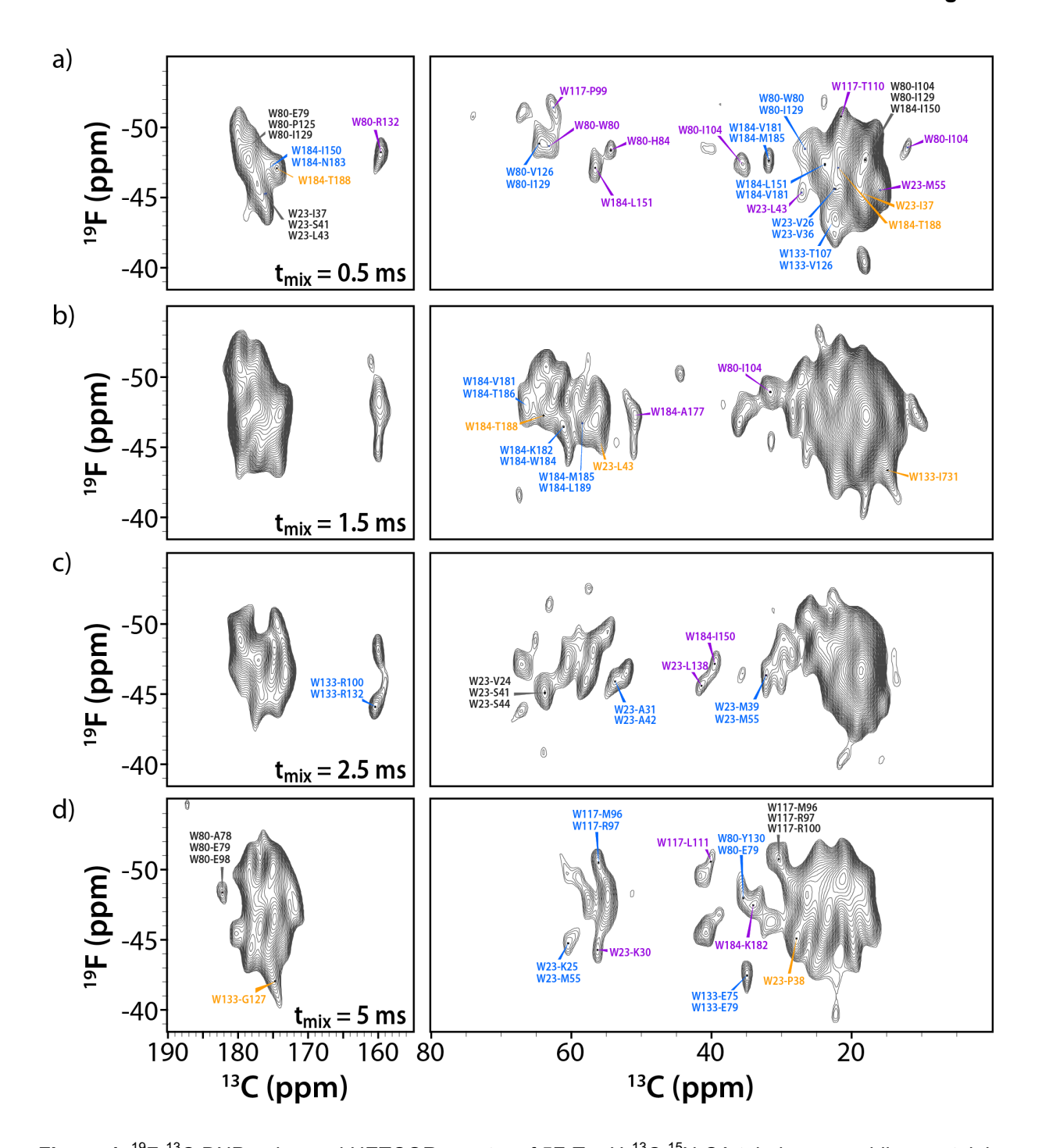


**Figure 4.** <sup>19</sup>F-<sup>13</sup>C DNP-enhanced HETCOR spectra of 5F-Trp,U-<sup>13</sup>C, <sup>15</sup>N CA tubular assemblies containing 15 mM AMUPol. The spectra were acquired at 14.1 T (564.8 MHz <sup>19</sup>F Larmor frequency) with a MAS frequency of 24 kHz. The mixing times are listed in each spectrum. Assignments of resolved cross peaks are shown in magenta, two-fold ambiguous assignments in blue, and assignments with 3-fold ambiguity in black. Tentative assignments of cross peaks in crowded regions of the spectrum based on the CA structure model are shown in orange. In the longer mixing time spectra (1.5, 2.5, and 5.0 ms) only peaks that are not

present in the shorter-mixing time data sets are labeled. The contour levels were set to 3.5 times the noise in all spectra.

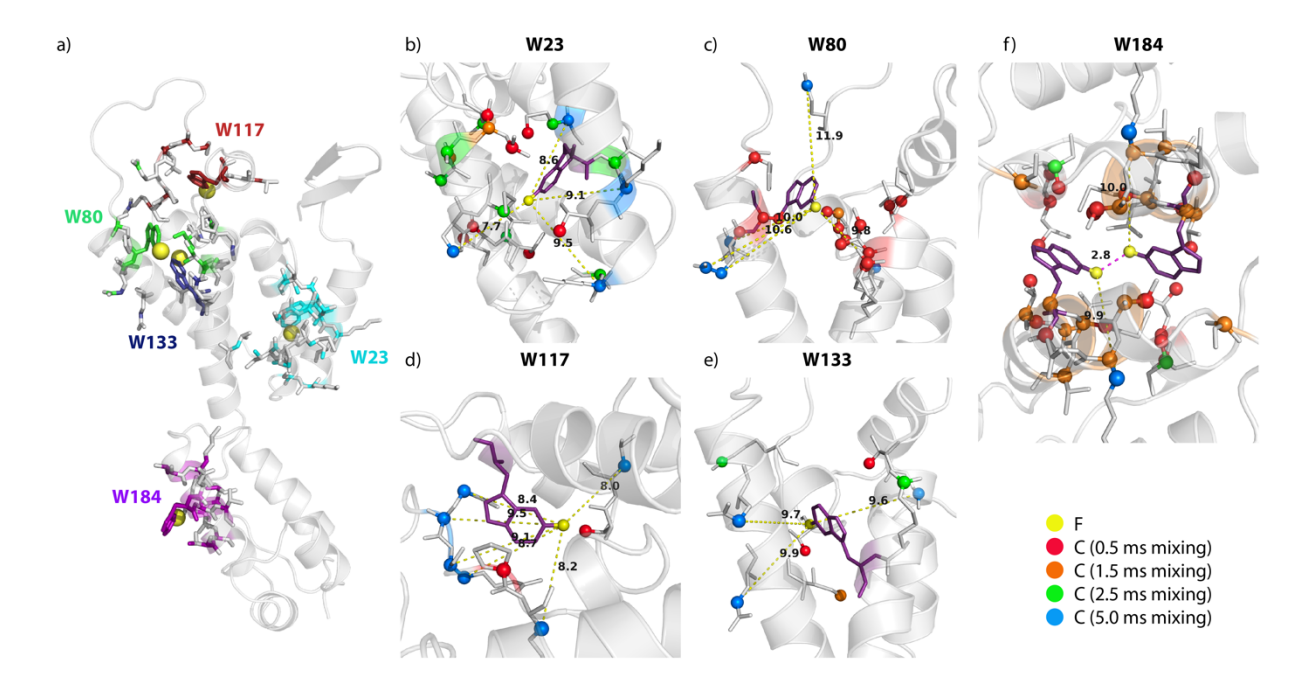


**Figure 5.** <sup>19</sup>F-<sup>13</sup>C contacts derived from DNP-enhanced HETCOR spectra of 5F-Trp,U-<sup>13</sup>C, <sup>15</sup>N CA tubular assemblies, mapped onto the a) CA monomer structure. Expansions are shown for b) W23, c) W80, d), W117, e) W133, and f) W184 dimer interface. Residues exhibiting correlations in the spectra are shown in stick representation and atoms associated with correlations that appear at different mixing times are color coded as follows: 0.5 ms (red), 1.5 ms (orange), 2.5 ms (green) and 5 ms (blue). Select distances in the range of 8-11 Å observed in the 5 ms mixing time spectra are shown by dashed lines.

## References

- (1) Quinn, C. M.; Polenova, T. *Q. Rev. Biophys.* **2017**, Structural Biology of Supramolecular Assemblies by Magic-Angle Spinning NMR Spectroscopy, *50*, e1.
- (2) Quinn, C. M.; Lu, M.; Suiter, C. L.; Hou, G.; Zhang, H.; Polenova, T. *Prog. Nucl. Magn. Reson. Spectrosc.* **2015**, Magic Angle Spinning NMR of Viruses, *86-87*, 21.
- (3) Bayro, M. J.; Chen, B.; Yau, W. M.; Tycko, R. *J. Mol. Biol.* **2014**, Site-Specific Structural Variations Accompanying Tubular Assembly of the HIV-1 Capsid Protein, *426*, 1109.
- (4) Wang, M.; Quinn, C. M.; Perilla, J. R.; Zhang, H.; Shirra, R., Jr.; Hou, G.; Byeon, I. J.; Suiter, C. L.; Ablan, S.; Urano, E.; Nitz, T. J.; Aiken, C.; Freed, E. O.; Zhang, P.; Schulten, K.; Gronenborn, A. M.; Polenova, T. *Nat. Commun.* **2017**, Quenching Protein Dynamics Interferes with HIV Capsid Maturation, *8*, 1779.
- (5) Yan, S.; Guo, C.; Hou, G.; Zhang, H.; Lu, X.; Williams, J. C.; Polenova, T. *Proc. Natl. Acad. Sci. USA* **2015**, Atomic-Resolution Structure of the CAP-Gly Domain of Dynactin on Polymeric Microtubules Determined by Magic Angle Spinning NMR Spectroscopy, *112*, 14611.
- (6) Yehl, J.; Kudryashova, E.; Reisler, E.; Kudryashov, D.; Polenova, T. *Scientific reports* **2017**, Structural Analysis of Human Cofilin 2/Filamentous Actin Assemblies: Atomic-Resolution Insights from Magic Angle Spinning NMR Spectroscopy, *7*, 44506.
- (7) Colvin, M. T.; Silvers, R.; Ni, Q. Z.; Can, T. V.; Sergeyev, I.; Rosay, M.; Donovan, K. J.; Michael, B.; Wall, J.; Linse, S.; Griffin, R. G. *J. Am. Chem. Soc.* **2016**, Atomic Resolution Structure of Monomorphic Abeta42 Amyloid Fibrils, *138*, 9663.
- (8) Qiang, W.; Yau, W. M.; Lu, J. X.; Collinge, J.; Tycko, R. *Nature* **2017**, Structural Variation in Amyloid-Beta Fibrils from Alzheimer's Disease Clinical Subtypes, *541*, 217.
- (9) Overhauser, A. W. Phys. Rev. 1953, Polarization of Nuclei in Metals, 92, 411.
- (10) Carver, T. R.; Slichter, C. P. *Phys. Rev.* **1953**, Polarization of Nuclear Spins in Metals, 92, 212.
- (11) Can, T. V.; Ni, Q. Z.; Griffin, R. G. *J. Magn. Reson.* **2015**, Mechanisms of Dynamic Nuclear Polarization in Insulating Solids, *253*, 23.
- (12) Lilly Thankamony, A. S.; Wittmann, J. J.; Kaushik, M.; Corzilius, B. *Prog. Nucl. Magn. Reson. Spectrosc.* **2017**, Dynamic Nuclear Polarization for Sensitivity Enhancement in Modern Solid-State NMR, *102-103*, 120.
- (13) Wenk, P.; Kaushik, M.; Richter, D.; Vogel, M.; Suess, B.; Corzilius, B. *J. Biomol. NMR* **2015**, Dynamic Nuclear Polarization of Nucleic Acid with Endogenously Bound Manganese, *63*, 97.
- (14) Maly, T.; Cui, D.; Griffin, R. G.; Miller, A.-F. *J. Phys. Chem. B* **2012**, <sup>1</sup>H Dynamic Nuclear Polarization Based on an Endogenous Radical, *116*, 7055.
- (15) Hu, K.-N.; Yu, H.-h.; Swager, T. M.; Griffin, R. G. *J. Am. Chem. Soc.* **2004**, Dynamic Nuclear Polarization with Biradicals, *126*, 10844.
- (16) Rosay, M.; Zeri, A.-C.; Astrof, N. S.; Opella, S. J.; Herzfeld, J.; Griffin, R. G. *J. Am. Chem. Soc.* **2001**, Sensitivity-Enhanced NMR of Biological Solids: Dynamic Nuclear Polarization of Y21M fd Bacteriophage and Purple Membrane, *123*, 1010.
- (17) Rosay, M.; Lansing, J. C.; Haddad, K. C.; Bachovchin, W. W.; Herzfeld, J.; Temkin, R. J.; Griffin, R. G. *J. Am. Chem. Soc.* **2003**, High-Frequency Dynamic Nuclear Polarization in MAS Spectra of Membrane and Soluble Proteins, *125*, 13626.
- (18) van der Wel, P. C. A.; Hu, K.-N.; Lewandowski, J.; Griffin, R. G. *J. Am. Chem. Soc.* **2006**, Dynamic Nuclear Polarization of Amyloidogenic Peptide Nanocrystals: GNNQQNY, a Core Segment of the Yeast Prion Protein Sup35p, *128*, 10840.
- (19) Bayro, M. J.; Debelouchina, G. T.; Eddy, M. T.; Birkett, N. R.; MacPhee, C. E.; Rosay, M.; Maas, W. E.; Dobson, C. M.; Griffin, R. G. *J. Am. Chem. Soc.* **2011**, Intermolecular Structure Determination of Amyloid Fibrils with Magic-Angle Spinning and Dynamic Nuclear Polarization NMR, *133*, 13967.

- (20) Koers, E. J.; López-Deber, M. P.; Weingarth, M.; Nand, D.; Hickman, D. T.; Mlaki Ndao, D.; Reis, P.; Granet, A.; Pfeifer, A.; Muhs, A.; Baldus, M. *Angew. Chem.* **2013**, Dynamic Nuclear Polarization NMR Spectroscopy: Revealing Multiple Conformations in Lipid-Anchored Peptide Vaccines, *52*, 10905.
- (21) Ravera, E.; Michaelis, V. K.; Ong, T.-C.; Keeler, E. G.; Martelli, T.; Fragai, M.; Griffin, R. G.; Luchinat, C. *ChemPhysChem* **2015**, Biosilica-Entrapped Enzymes can be studied by DNP-enhanced high-field NMR, *16*, 2751.
- (22) Viger-Gravel, J.; Schantz, A.; Pinon, A. C.; Rossini, A. J.; Schantz, S.; Emsley, L. *J. Phys. Chem. B* **2018**, Structure of Lipid Nanoparticles Containing siRNA or mRNA by Dynamic Nuclear Polarization-Enhanced NMR Spectroscopy, *122*, 2073.
- (23) Viennet, T.; Viegas, A.; Kuepper, A.; Arens, S.; Gelev, V.; Petrov, O.; Grossmann, T. N.; Heise, H.; Etzkorn, M. *Angew. Chem.* **2016**, Selective Protein Hyperpolarization in Cell Lysates Using Targeted Dynamic Nuclear Polarization, *55*, 10746.
- (24) Albert, B. J.; Gao, C.; Sesti, E. L.; Saliba, E. P.; Alaniva, N.; Scott, F. J.; Sigurdsson, S. T.; Barnes, A. B. *Biochemistry* **2018**, Dynamic Nuclear Polarization Nuclear Magnetic Resonance in Human Cells Using Fluorescent Polarizing Agents.
- (25) Gupta, R.; Lu, M.; Hou, G.; Caporini, M. A.; Rosay, M.; Maas, W.; Struppe, J.; Suiter, C.; Ahn, J.; Byeon, I.-J. L.; Franks, W. T.; Orwick-Rydmark, M.; Bertarello, A.; Oschkinat, H.; Lesage, A.; Pintacuda, G.; Gronenborn, A. M.; Polenova, T. *J. Phys. Chem. B* **2016**, Dynamic Nuclear Polarization Enhanced MAS NMR Spectroscopy for Structural Analysis of HIV-1 Protein Assemblies, *120*, 329.
- (26) Jaudzems, K.; Bertarello, A.; Chaudhari, S. R.; Pica, A.; Cala-De Paepe, D.; Barbet-Massin, E.; Pell, A. J.; Akopjana, I.; Kotelovica, S.; Gajan, D.; Ouari, O.; Tars, K.; Pintacuda, G.; Lesage, A. *Angew. Chem.* **2018**, Dynamic Nuclear Polarization-Enhanced Biomolecular NMR Spectroscopy at High Magnetic Field with Fast Magic-Angle Spinning, *57*, 7458.
- (27) Daube, D.; Aladin, V.; Heiliger, J.; Wittmann, J. J.; Barthelmes, D.; Bengs, C.; Schwalbe, H.; Corzilius, B. *J. Am. Chem. Soc.* **2016**, Heteronuclear Cross-Relaxation under Solid-State Dynamic Nuclear Polarization, *138*, 16572.
- (28) Wylie, B. J.; Dzikovski, B. G.; Pawsey, S.; Caporini, M.; Rosay, M.; Freed, J. H.; McDermott, A. E. *J. Biomol. NMR* **2015**, Dynamic Nuclear Polarization of Membrane Proteins: Covalently Bound Spin-Labels at Protein-Protein Interfaces, *61*, 361.
- (29) Akbey, Ü.; Franks, W. T.; Linden, A.; Lange, S.; Griffin, R. G.; van Rossum, B.-J.; Oschkinat, H. *Angew. Chem.* **2010**, Dynamic Nuclear Polarization of Deuterated Proteins, *49*, 7803.
- (30) Geiger, M.-A.; Orwick-Rydmark, M.; Märker, K.; Franks, W. T.; Akhmetzyanov, D.; Stöppler, D.; Zinke, M.; Specker, E.; Nazaré, M.; Diehl, A.; van Rossum, B.-J.; Aussenac, F.; Prisner, T.; Akbey, Ü.; Oschkinat, H. *PhysChemChemPhys* **2016**, Temperature Dependence of Cross-Effect Dynamic Nuclear Polarization in Rotating Solids: Advantages of Elevated Temperatures, *18*, 30696.
- (31) Barnes, A. B.; Corzilius, B.; Mak-Jurkauskas, M. L.; Andreas, L. B.; Bajaj, V. S.; Matsuki, Y.; Belenky, M. L.; Lugtenburg, J.; Sirigiri, J. R.; Temkin, R. J.; Herzfeld, J.; Griffin, R. G. *PhysChemChemPhys* **2010**, Resolution and Polarization Sistribution in Cryogenic DNP/MAS Experiments, *12*, 5861.
- (32) Fricke, P.; Mance, D.; Chevelkov, V.; Giller, K.; Becker, S.; Baldus, M.; Lange, A. *J. Biomol. NMR* **2016**, High Resolution Observed in 800 MHz DNP Spectra of Extremely Rigid Type III Secretion Needles, *65*, 121.
- (33) Bouleau, E.; Saint-Bonnet, P.; Mentink-Vigier, F.; Takahashi, H.; Jacquot, J. F.; Bardet, M.; Aussenac, F.; Purea, A.; Engelke, F.; Hediger, S.; Lee, D.; De Paëpe, G. *Chem. Sci.* **2015**, Pushing NMR Sensitivity Limits Using Dynamic Nuclear Polarization with Closed-Loop Cryogenic Helium Sample Spinning, *6*, 6806.

- (34) Linden, A. H.; Franks, W. T.; Akbey, U.; Lange, S.; van Rossum, B. J.; Oschkinat, H. *J. Biomol. NMR* **2011**, Cryogenic Temperature Effects and Resolution upon Slow Cooling of Protein Preparations in Solid State NMR, *51*, 283.
- (35) Rogawski, R.; Sergeyev, I. V.; Zhang, Y.; Tran, T. H.; Li, Y. J.; Tong, L.; McDermott, A. E. *J. Phys. Chem. B* **2017**, NMR Signal Quenching from Bound Biradical Affinity Reagents in DNP Samples, *121*, 10770.
- (36) Ganser-Pornillos, B. K.; von Schwedler, U. K.; Stray, K. M.; Aiken, C.; Sundquist, W. I. *J. Virol.* **2004**, Assembly Properties of the Human Immunodeficiency Virus Type 1 CA Protein, *78*, 2545.
- (37) Byeon, I. J. L.; Hou, G. J.; Han, Y.; Suiter, C. L.; Ahn, J.; Jung, J.; Byeon, C. H.; Gronenborn, A. M.; Polenova, T. *J. Am. Chem. Soc.* **2012**, Motions on the Mllisecond Time Scale and Multiple Conformations of HIV-1 Capsid Protein: Implications for Structural Polymorphism of CA Assemblies, *134*, 6455.
- (38) Han, Y.; Hou, G. J.; Suiter, C. L.; Ahn, J.; Byeon, I. J. L.; Lipton, A. S.; Burton, S.; Hung, I.; Gor'kov, P. L.; Gan, Z. H.; Brey, W.; Rice, D.; Gronenborn, A. M.; Polenova, T. *J. Am. Chem. Soc.* **2013**, Magic Angle Spinning NMR Reveals Sequence-Dependent Structural Plasticity, Dynamics, and the Spacer Peptide 1 Conformation in HIV-1 Capsid Protein Assemblies, *135*, 17793.
- (39) Lu, M.; Hou, G.; Zhang, H.; Suiter, C. L.; Ahn, J.; Byeon, I. J.; Perilla, J. R.; Langmead, C. J.; Hung, I.; Gor'kov, P. L.; Gan, Z.; Brey, W.; Aiken, C.; Zhang, P.; Schulten, K.; Gronenborn, A. M.; Polenova, T. *Proc. Natl. Acad. Sci. USA* **2015**, Dynamic Allostery Governs Cyclophilin A-HIV Capsid Interplay, *112*, 14617.
- (40) Zhang, H.; Hou, G.; Lu, M.; Ahn, J.; Byeon, I. L.; Langmead, C. J.; Perilla, J. R.; Hung, I.; Gor'kov, P. L.; Gan, Z.; Brey, W. W.; Case, D. A.; Schulten, K.; Gronenborn, A. M.; Polenova, T. *J. Am. Chem. Soc.* **2016**, HIV-1 Capsid Function is Regulated by Dynamics: Quantitative Atomic-Resolution Insights by Integrating Magic-Angle-Spinning NMR, QM/MM, and MD, *138*, 14066.
- (41) Bayro, M. J.; Tycko, R. *J. Am. Chem. Soc.* **2016**, Structure of the Dimerization Interface in the Mature HIV-1 Capsid Protein Lattice from Solid State NMR of Tubular Assemblies, *138*, 8538.
- (42) Byeon, I. J. L.; Meng, X.; Jung, J. W.; Zhao, G. P.; Yang, R. F.; Ahn, J. W.; Shi, J.; Concel, J.; Aiken, C.; Zhang, P. J.; Gronenborn, A. M. *Cell* **2009**, Structural Convergence between Cryo-EM and NMR Reveals Intersubunit Interactions Critical for HIV-1 Capsid Function, *139*, 780.
- (43) Zhao, G. P.; Perilla, J. R.; Yufenyuy, E. L.; Meng, X.; Chen, B.; Ning, J. Y.; Ahn, J.; Gronenborn, A. M.; Schulten, K.; Aiken, C.; Zhang, P. J. *Nature* **2013**, Mature HIV-1 Capsid Structure by Cryo-Electron Microscopy and All-Atom Molecular Dynamics, *4*97, 643.
- (44) Zhang, P.; Meng, X.; Zhao, G. *Methods Mol. Biol.* **2013**, Tubular Crystals and Helical Arrays: Structural Determination of HIV-1 Capsid Assemblies Using Iterative Helical Real-Space Reconstruction, *955*, 381.
- (45) Wang, M.; Lu, M.; Fritz, M.; Quinn, C.; Byeon, I. J.; Byeon, C. H.; Struppe, J.; Maas, W.; Gronenborn, A.; Polenova, T. *Angew. Chem.* **2018**, Fast Magic Angle Spinning <sup>19</sup>F NMR of HIV-1 Capsid Protein Assemblies.
- (46) Holl, S. M.; Marshall, G. R.; Beusen, D. D.; Kociolek, K.; Redlinski, A. S.; Leplawy, M. T.; McKay, R. A.; Vega, S.; Schaefer, J. *J. Am. Chem. Soc.* **1992**, Deteremination of an 8-Angstrom Interatomic Distance in a Helical Peptide by Solid-State NMR Spectroscopy, *114*, 4830.
- (47) Afonin, S.; Kubyslikin, V.; Mykhailiuk, P. K.; Komarov, I. V.; Ulrich, A. S. *J. Phys. Chem. B* **2017**, Conformational Plasticity of the Cell-Penetrating Peptide SAP As Revealed by Solid-State F-19-NMR and Circular Dichroism Spectroscopies, *121*, 6479.
- (48) Koch, K.; Afonin, S.; Ieronimo, M.; Berditsch, M.; Ulrich, A. S. In *Solid State NMR*; Chan, J. C. C., Ed. 2012; Vol. 306, p 89.

- (49) Elkins, M. R.; Williams, J. K.; Gelenter, M. D.; Dai, P.; Kwon, B.; Sergeyev, I. V.; Pentelute, B. L.; Hong, M. *Proc. Natl. Acad. Sci. U. S. A.* **2017**, Cholesterol-Binding Site of the Influenza M2 Protein in Lipid Bilayers from Solid-State NMR, *114*, 12946.
- (50) Roos, M.; Mandala, V. S.; Hong, M. *J. Phys. Chem. B* **2018**, Determination of Long-Range Distances by Fast Magic-Angle-Spinning Radiofrequency-Driven <sup>19</sup>F-<sup>19</sup>F Dipolar Recoupling NMR.
- (51) Roos, M.; Wang, T.; Shcherbakov, A. A.; Hong, M. *J. Phys. Chem. B* **2018**, Fast Magic-Angle-Spinning <sup>19</sup>F Spin Exchange NMR for Determining Nanometer <sup>19</sup>F-<sup>19</sup>F Distances in Proteins and Pharmaceutical Compounds, *122*, 2900.
- (52) Lu, M.; Sarkar, S.; Wang, M.; Kraus, J.; Fritz, M.; Quinn, C. M.; Bai, S.; Holmes, S. T.; Dybowski, C.; Yap, G. P. A.; Struppe, J.; Sergeyev, I. V.; Maas, W.; Gronenborn, A. M.; Polenova, T. *J. Phys. Chem. B* **2018**, <sup>19</sup>F Magic Angle Spinning NMR Spectroscopy and Density Functional Theory Calculations of Fluorosubstituted Tryptophans: Integrating Experiment and Theory for Accurate Determination of Chemical Shift Tensors.
- (53) Sauvée, C.; Rosay, M.; Casano, G.; Aussenac, F.; Weber, R. T.; Ouari, O.; Tordo, P. *Angew. Chem.* **2013**, Highly Efficient, Water-Soluble Polarizing Agents for Dynamic Nuclear Polarization at High Frequency, *52*, 10858.
- (54) Crowley, P. B.; Kyne, C.; Monteith, W. B. *Chem. Commun.* **2012**, Simple and Inexpensive Incorporation of <sup>19</sup>F-Tryptophan for Protein NMR Spectroscopy, *48*, 10681.
- (55) Sun, S. J.; Han, Y.; Paramasivam, S.; Yan, S.; Siglin, A. E.; Williams, J. C.; Byeon, I. J. L.; Ahn, J.; Gronenborn, A. M.; Polenova, T. *Methods. Mol. Biol.* **2012**, Solid-State NMR Spectroscopy of Protein Complexes, *831*, 303.
- (56) Thurber, K. R.; Tycko, R. *J. Magn. Reson.* **2009**, Measurement of Sample Temperatures Under Magic-Angle Spinning from the Chemical Shift and Spin-Lattice Relaxation Rate of <sup>79</sup>Br in KBr Powder, *196*, 84.
- (57) Bennett, A. E.; Rienstra, C. M.; Griffiths, J. M.; Zhen, W.; Lansbury, P. T. J.; Griffin, R. G. *J. Chem. Phys.* **1998**, Homonuclear Radio Frequency-Driven Recoupling in Rotating Solids, *108*. 9463.
- (58) Bennett, A. E.; Rienstra, C. M.; Auger, M.; Lakshmi, K. V.; Griffin, R. G. *J. Chem. Phys.* **1995**, Heteronuclear Decoupling in Rotating Solids, *103*, 6951.
- (59) Maurer, T.; Kalbitzer, H. R. *J. Magn. Reson. Ser. B* **1996**, Indirect Referencing of P-31 and F-19 NMR Spectra, *113*, 177.
- (60) Marion, D.; Ikura, M.; Tschudin, R.; Bax, A. *J. Magn. Reson.* **1989**, Rapid recording of 2D NMR spectra without phase cycling. Application to the study of hydrogen exchange in proteins, *85*, 393.
- (61) Delaglio, F.; Grzesiek, S.; Vuister, G. W.; Zhu, G.; Pfeifer, J.; Bax, A. *J. Biomol. NMR* **1995**, NMRPipe: A Multidimensional Spectral Processing System Based on UNIX Pipes, *6*, 277. (62) Author SPARKY 3, Institution, 2004.
- (63) Mentink-Vigier, F.; Akbey, Ü.; Oschkinat, H.; Vega, S.; Feintuch, A. *J. Magn. Reson.* **2015**, Theoretical aspects of Magic Angle Spinning Dynamic Nuclear Polarization, *258*, 102.
- (64) Chaudhari, S. R.; Berruyer, P.; Gajan, D.; Reiter, C.; Engelke, F.; Silverio, D. L.; Copéret, C.; Lelli, M.; Lesage, A.; Emsley, L. *PhysChemChemPhys* **2016**, Dynamic nuclear polarization at 40 kHz magic angle spinning †Electronic supplementary information (ESI) available: Experimental details, with supplementary tables and figures. See DOI: 10.1039/c6cp00839a Click here for additional data file, *18*, 10616.
- (65) Mentink-Vigier, F.; Mathies, G.; Liu, Y.; Barra, A.-L.; Caporini, M. A.; Lee, D.; Hediger, S.; G. Griffin, R.; De Paëpe, G. *Chem. Sci.* **2017**, Efficient Cross-Effect Dynamic Nuclear Polarization Without Depolarization in High-Resolution MAS NMR, *8*, 8150.
- (66) Thurber, K. R.; Tycko, R. *J. Chem. Phys.* **2012**, Theory for Cross Effect Dynamic Nuclear Polarization under Magic-Angle Spinning in Ssolid State Nuclear Magnetic Resonance: The Importance of Level Crossings, *137*, 084508.

- (67) Chaudhari, S. R.; Wisser, D.; Pinon, A. C.; Berruyer, P.; Gajan, D.; Tordo, P.; Ouari, O.; Reiter, C.; Engelke, F.; Copéret, C.; Lelli, M.; Lesage, A.; Emsley, L. *J. Am. Chem. Soc.* **2017**, Dynamic Nuclear Polarization Efficiency Increased by Very Fast Magic Angle Spinning, *139*, 10609.
- (68) Lange, S.; Linden, A. H.; Akbey, Ü.; Trent Franks, W.; Loening, N. M.; Rossum, B.-J. v.; Oschkinat, H. *J. Magn. Reson.* **2012**, The Effect of Biradical Concentration on the Performance of DNP-MAS-NMR, *216*, 209.
- (69) Viger-Gravel, J.; Avalos, C. E.; Kubicki, D. J.; Lelli, M.; Ouari, O.; Lesage, A.; Emsley, L. In 59th Rocky Mountain Conference on Magnetic Resonance Snowbird, UT, July 22-27, 2018, p 111.
- (70) Takahashi, H.; Lee, D.; Dubois, L.; Bardet, M.; Hediger, S.; De Paëpe, G. *Angew. Chem.* **2012**, Rapid Natural-Abundance 2D 13C–13C Correlation Spectroscopy Using Dynamic Nuclear Polarization Enhanced Solid-State NMR and Matrix-Free Sample Preparation, *51*, 11766.
- (71) He, L.; Bardiaux, B.; Ahmed, M.; Spehr, J.; Konig, R.; Lunsdorf, H.; Rand, U.; Luhrs, T.; Ritter, C. *Proc. Natl. Acad. Sci. USA* **2016**, Structure Determination of Helical Filaments by Solid-State NMR Spectroscopy, *113*, E272.
- (72) Retel, J. S.; Nieuwkoop, A. J.; Hiller, M.; Higman, V. A.; Barbet-Massin, E.; Stanek, J.; Andreas, L. B.; Franks, W. T.; van Rossum, B. J.; Vinothkumar, K. R.; Handel, L.; de Palma, G. G.; Bardiaux, B.; Pintacuda, G.; Emsley, L.; Kuhlbrandt, W.; Oschkinat, H. *Nat. Commun.* **2017**, Structure of Outer Membrane Protein G in Lipid Bilayers, *8*, 2073.
- (73) Shi, C.; Fricke, P.; Lin, L.; Chevelkov, V.; Wegstroth, M.; Giller, K.; Becker, S.; Thanbichler, M.; Lange, A. *Sci. Adv.* **2015**, Atomic-Resolution Structure of Cytoskeletal Bactofilin by Solid-State NMR, *1*, e1501087.
- (74) Tuttle, M. D.; Comellas, G.; Nieuwkoop, A. J.; Covell, D. J.; Berthold, D. A.; Kloepper, K. D.; Courtney, J. M.; Kim, J. K.; Barclay, A. M.; Kendall, A.; Wan, W.; Stubbs, G.; Schwieters, C. D.; Lee, V. M.; George, J. M.; Rienstra, C. M. *Nat. Struct. Mol. Biol.* **2016**, Solid-State NMR Structure of a Pathogenic Fibril of Full-Length Human Alpha-Synuclein, *23*, 409.
- (75) Zech, S. G.; Wand, A. J.; McDermott, A. E. *J. Am. Chem. Soc.* **2005**, Protein Structure Determination by High-Resolution Solid-State NMR Spectroscopy: Application to Microcrystalline Ubiquitin, *127*, 8618.

# TOC Graphic

